24 April 1998

ELSEVIER

Chemical Physics Letters 287 (1998) 209–215

CHEMICAL PHYSICS LETTERS

# Weak interactions and photoinitiated unimolecular decomposition

K. Mikhaylichenko, C. Wittig

*Department of Chemistry, University of Southern California, Los Angeles, CA 90089-0482, USA*

Received 30 December 1997; in final form 26 January 1998

**Abstract**

Numerical studies have been carried out to examine the applicability of the density of states measured just below dissociation threshold to transition state rate theory. The model system consists of two weakly interacting manifolds of levels, one of which is optically accessible. Both manifolds are coupled to dissociative continua. These studies demonstrate that immediately above reaction threshold, coupling to continua is relatively slow on the time scale of inter-manifold coupling, and it is the mixed manifolds which decay. At higher energies, couplings to continua exceed inter-manifold couplings, and it is the photoexcited bright states which undergo unimolecular decomposition. 

## 1. Introduction

Densities of states are central to transition state theories of unimolecular decomposition in which the rate is expressed as:

$$k_{\mathrm{TST}} = \frac{N^{\ddagger}(E - E_0)}{h\rho(E)} \qquad (1)$$

where $N^{\ddagger}(E - E_0)$ is the number of open channels at the transition state and $\rho(E)$ is the density of states for the reactant part of the system [1,2]. Since statistical behavior is a manifestation of complex quantum dynamics [3], inferring $\rho(E)$ values from experiments (e.g. high-resolution spectroscopy) requires care. For example, one must consider symmetries, optical selection rules, and the simultaneous participation of multiple potential energy surfaces (PES) in order to establish the nature of the optically accessible states which undergo photoinitiated decomposition. Consequently, important issues have arisen which include: (i) relating the density of optical transitions that terminate on levels just below dissociation threshold ($D_0$) to the densities of vibronic and rovibronic levels and (ii) what is the most appropriate description of the levels (from immediately above to well-above $D_0$) that are sampled by the wavepacket during photoinitiated unimolecular decomposition.

Polyatomic molecules provide hierarchies of coupling strengths, with strong couplings giving rise to fast dynamics and coarse spectral features, and weaker couplings giving rise to longer time scales and finer spectral structure. The energy region near $D_0$ often provides information about the latter, e.g. breakdown of approximate symmetries, rovibronic chaos, participation of multiple PESs, etc. The present work focuses on this regime.

A good example is $NO_2$. Conical intersection and strong nonadiabatic interaction between the $X\,^2A_2$ and $A\,^2B_2$ electronic states leads to vibronic chaos $\sim 10000\ \mathrm{cm}^{-1}$ below $D_0$ [4–7]. This gives rise to $A_1$ and $B_2$ vibronic species [4], with only $B_2$ being optically accessible from the ground state. In addition, $A_1$ and $B_2$ vibronic species are mixed through

0009-2614/98/$19.00 
PII: S0009-2614(98)00164-X

relatively weak spin–rotation and Coriolis interactions, and rovibronic chaos has been reported well below $D_0$ [8]. In addition, it has been found that the density of spectroscopically accessible vibronic levels increases dramatically within 2.5 $cm^{-1}$ of $D_0$. Namely, the measured value is $5.4/cm^{-1}$ [9], whereas the extrapolated value for combined $A_1$ and $B_2$ vibronic species is $0.77/cm^{-1}$ [10]. This phenomenon is not well understood. Most importantly, it is not clear that the physics that leads to the high density of states observed just below $D_0$ is important at energies in excess of $D_0$.

Many recent studies of high vibrational levels of polyatomic molecules deal with the issues of chaos and statistical behavior in molecular systems. Due to complicated quantum mechanical behavior, the levels are often best treated by using statistical theories which describe the general appearance and the degree of irregularity of the level structure, rather than by detailed examination of individual levels [11,12]. A large body of literature has dealt with distributions of level spacings for a variety of spectra and level structures [13–15]. Moreover, their statistical properties have been used as measures of quantum ergodicity [16–18]. Work on formaldehyde [19] and acetylene [18,20] provide good background.

In this Letter, the relationship between $\rho(E)$ measured just below $D_0$ and the $\rho(E)$ used in Eq. (1) is discussed. Numerical experiments are carried out for a model system that resembles $NO_2$. Fig. 1 shows two isoenergetic manifolds of levels: optically accessible (bright) and optically inaccessible (dark). The

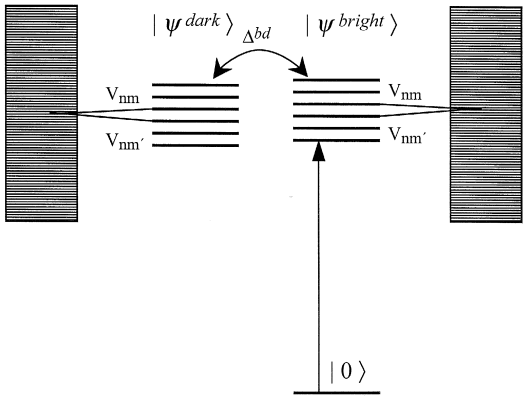


Fig. 1. The coupling scheme.

manifolds are weakly coupled and each manifold is coupled to its own dissociation continuum. For the case of $NO_2$, the inter-manifold coupling is due to spin–rotation and Coriolis interactions. To generate the bright and dark levels the random matrix version of the optical model is used. Statistical properties of the levels are used to illustrate the interplay between coupling to continua and inter-manifold coupling. Just above $D_0$ the resonances are of mixed $A_1/B_2$ vibronic character, and it is shown that at higher energies (i.e. when the reaction rates exceed the $A_1/B_2$ coupling rates), the photoexcited $B_2$ bright states decay before they can couple to nearby $A_1$ levels.

## 2. Overview of level spacing statistics

Nuclear motions of molecules having high vibrational excitation (below bond dissociation energies) are nearly always irregular. In this regime the levels are correlated (i.e. zeroth-order levels repel each other) and display the statistical properties of a Gaussian orthogonal ensemble (GOE) of real symmetric matrices [13]. For example, distributions of adjacent level spacings ($s$) agree well with the GOE prediction, which is almost identical to the Wigner formula [21]:

$$P_{\mathrm{Wigner}}(s) = \frac{\pi}{2}\frac{s}{\langle s\rangle^2}\exp\left(-\frac{\pi}{4}\frac{s^2}{\langle s\rangle^2}\right) \qquad (2)$$

where $\langle s\rangle$ is the mean level spacing. On the other hand, in a regular system the levels are not correlated and lie randomly with respect to each other, displaying Poisson statistics [22]:

$$P_{\mathrm{Poisson}}(s) = \frac{1}{\langle s\rangle}\exp\left(-\frac{s}{\langle s\rangle}\right). \qquad (3)$$

With two or more manifolds present the situation is more complex. For example, the distribution obtained by superposing just two Wigner distributions is distinctly non-zero at the origin [14]. Such behavior is characteristic of mixed sequences, which result from random superpositions of non-interacting manifolds.

The statistical properties of discrete spectra differ from those of reactive resonances, since the eigen-

values of the former lie on the real axis while those of the latter lie in the complex plane [23,24]. In chaotic systems, reactive resonances follow the statistical law of a Gaussian ensemble of complex symmetric (non-Hermitian) matrices, developed by Ginibre [25].

$$P^{2D}_{\text{Ginibre}}(s) = 2\left(\frac{9\pi}{16}\right)^2 \frac{s^3}{\langle s\rangle^4}\exp\left(-\frac{9\pi}{16}\frac{s^2}{\langle s\rangle^2}\right) \quad (4)$$

where 2D denotes the complex plane, and $s$ is now the magnitude of the nearest-neighbor spacing in the complex plane. Analogous to Eq. (3), an ensemble of uncorrelated random numbers distributed uniformly in a plane is described by the distribution:

$$P^{2D}_{\text{Poisson}}(s) = \frac{\pi}{2}\frac{s}{\langle s\rangle^2}\exp\left(-\frac{\pi}{4}\frac{s^2}{\langle s\rangle^2}\right). \quad (5)$$

It is easier to distinguish between the Wigner and Poisson distributions for bound levels given by Eqs. (2) and (3) than between the Ginibre and Poisson distributions for reactive resonances given by Eqs. (4) and (5). In the regime of reactive resonances the statistics should be carried out using the complex energies. However, only in rare cases are the resonances sufficiently isolated that such data can be obtained experimentally.

## 3. The model

Fig. 1 shows manifolds of optically accessible levels $|\psi^{\text{bright}}\rangle$ and optically inaccessible levels $|\psi^{\text{dark}}\rangle$. The manifolds are coupled to each other as well as to their respective continua. Each manifold is described with an effective Hamiltonian [26], $H^{\text{eff}}$, by using a random matrix version of the optical model [27–30]. For each manifold, the Hilbert space is partitioned into two subspaces (i.e. discrete molecular states and dissociative continua), and the matrix elements are given by:

$$H^{\text{eff}}_{m,m'} = E_m\delta_{m,m'} - i\pi\sum_{n=1}^{N} V_{m,n}V_{n,m'} \quad (6)$$

where the maximum value of $m(m')$ is $M$, the number of states in each discrete space, and $N$ is the number of independent decay channels. The width matrix is given by:

$$\hbar\Gamma_{m,m'} = 2\pi\sum_{n=1}^{N} V_{m,n}V_{n,m'}. \quad (7)$$

Within each manifold, $E_m$ values are drawn randomly from a Wigner distribution and the $V_{m,n}$ are drawn randomly from a Gaussian distribution with zero mean and standard deviation, $\sigma$:

$$\sigma^2 = \frac{1}{MN}\sum_{m=1}^{M}\sum_{n=1}^{N} V_{nm}^2. \quad (8)$$

Thus, the average value of the diagonal elements of the width matrix is given by $\langle\Gamma\rangle = 2\pi N\sigma^2$, and $\langle\bar{\Gamma}\rangle$ is the average value of the width matrix further averaged over the random matrix ensemble. Inter-manifold coupling via the discrete states is introduced through real matrix elements, $\Delta^{\text{bd}}$, which are chosen as independent identically distributed random variables with zero mean and variance $\sigma_{\text{bd}}$, i.e. $\langle\Delta^{\text{bd}}\rangle = 0$ and $\sqrt{\langle\Delta^2_{\text{bd}}\rangle} = \sigma_{\text{bd}}$. Thus, the $H^{\text{eff}}$ matrix has the form:

$$\begin{bmatrix} E_m^{\text{bright}} - i\dfrac{\hbar\Gamma^{\text{bright}}_{m,m'}}{2} & \Delta^{\text{bd}} \\ \Delta^{\text{bd}} & E_m^{\text{dark}} - i\dfrac{\hbar\Gamma^{\text{dark}}_{m,m'}}{2} \end{bmatrix}. \quad (9)$$

As written the matrix is not energy ordered, since the bright and dark manifolds cover the same energy range. The model is applicable in a small energy interval since it does not incorporate the energy dependence of the mean density of states and the average resonance width.

## 4. Results and discussion

The complex energy eigenvalues were obtained by diagonalizing $H^{\text{eff}}$ for a given random selection of matrix elements. These eigenvalues were used to construct level-spacing distributions, $P(s)$. Averaging $P(s)$ over the random matrix ensemble was achieved by repeating this for different random selections of matrix elements. Densities of states were set at $\rho_{\text{bright}} = \rho_{\text{dark}} = 0.5/\text{cm}^{-1}$, giving a mean spacing of unity for the combined manifolds. The numbers of discrete levels were set at $M_{\text{bright}} = M_{\text{dark}}$

$= 125$, and the numbers of independent open channels were set at $N_{\text{bright}} = N_{\text{dark}} = 15$.

Inter-manifold coupling in the absence of coupling to continua was checked by nulling the width matrix. Fig. 2 shows $P(s)$ distributions for different values of $\sigma_{\text{bd}}$. Fig. 2a gives $P(s)$ for the diagonal elements of the effective Hamiltonian matrix ($\sigma_{\text{bd}} = 0$). Note that although energies within each manifold were drawn from a Wigner distribution, $P(s) \neq 0$ at $s = 0$, since inter-manifold coupling is zero. On the other hand, Wigner-like distributions are obtained when $\sigma_{\text{bd}}$ is at least comparable to the average level spacing, as shown in Fig. 2c,d.

Next, effects due to the finite size of the matrix were checked by examining $\rho(E)$, which should not depend upon the strength of the couplings. With the present matrix representation, strong couplings push some levels out of the original energy interval, thus decreasing $\rho(E)$. As seen from Fig. 3, these effects begin to be significant at $\sigma_{\text{bd}} \sim 5$. Therefore, the calculations presented below were done with $\sigma_{\text{bd}} = 2$. Referring to Fig. 2, this choice provides enough inter-manifold coupling to ensure Wigner-like behavior in the absence of coupling to continua.

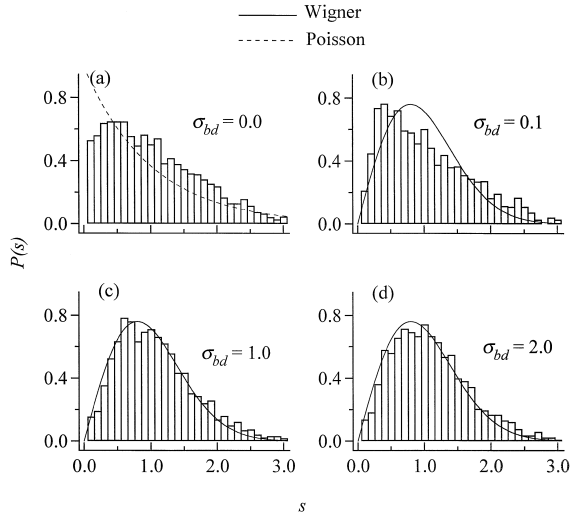


Fig. 2. Nearest-neighbor spacing distributions, $P(s)$, for two coupled manifolds of bound states with different values of $\sigma_{\text{bd}}$. Also shown are Wigner (————) and 1D Poisson (- - -) distributions, corresponding to chaotic and regular bound systems, respectively.

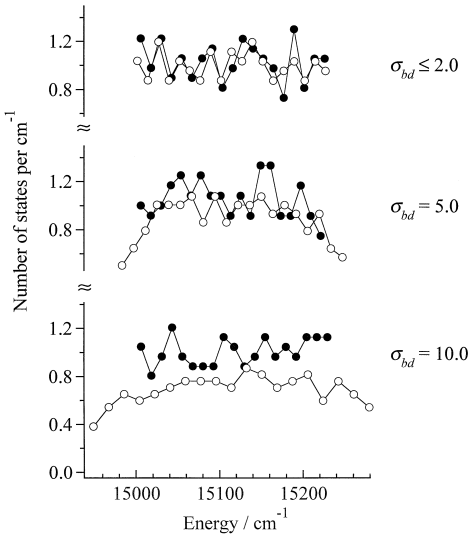


Fig. 3. Density of states for two coupled manifolds of bound states. ●, Diagonal elements of $H^{\text{eff}}$, i.e. before diagonalization; ○, eigenstates after diagonalization. The lines are to guide the eye.

$P(s)$ distributions, where $s$ is now the nearest-neighbor distance in the complex energy plane, are shown in Fig. 4 for $\langle \bar{\Gamma} \rangle \rho = 5.0$. To obtain these, the distributions were unfolded, i.e. uniformly distributed in the complex plane with unit mean spacing [31]. Fig. 4 a shows $P(s)$ for a single manifold along with $P_{\text{Ginibre}}(s)$ (solid line), which fits pretty well. $P(s)$ for the superposition of two uncoupled manifolds is shown in Fig. 4b, together with $P_{\text{Ginibre}}(s)$ (solid line) and $P^{2D}_{\text{Ginibre}}(s)$ (dashed line). As mentioned earlier, $P(s)$ lies between these two limiting curves when two non-interacting manifolds are superimposed. However, the solid and dashed curves do not differ enough to provide a reliable test.

Competition between inter-manifold coupling and coupling to continua is revealed in Fig. 5, which shows $P(s_{\text{re}})$ distributions for one manifold (upper row) and two coupled manifolds with $\sigma_{\text{bd}} = 2.0$ (lower row). In this case, $s_{\text{re}}$ is the real part of the resonance energy.

For the case of one manifold, increasing the coupling to the continuum results in $P(s_{\text{re}})$ evolving from $P_{\text{Wigner}}(s_{\text{re}})$ toward $P_{\text{Poisson}}(s_{\text{re}})$, as expected (Fig. 5a–c). For this one-manifold case, the energy

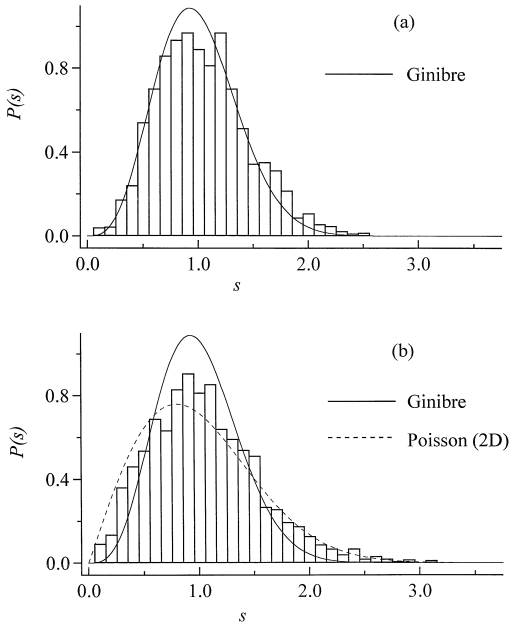


Fig. 4. Nearest-neighbor spacing distributions in the complex energy plane, $P(s)$, for resonances with $\langle \bar{\Gamma} \rangle \rho = 5.0$ for (a) one manifold and (b) a superposition of two uncorrelated manifolds, i.e. $\sigma_{bd} = 0.0$. Also shown are the Ginibre (————) and 2D Poisson (---) distributions for chaotic and regular ensembles of reactive resonances, respectively.

levels $E_m$, which serve as input parameters to the model Hamiltonian, were drawn from a Wigner distribution. Therefore, one expects the distribution of the real parts of the eigenvalues, $P(s_{re})$, to follow the Wigner distribution as long as coupling to the continuum is weak. For example, $\langle \bar{\Gamma} \rangle \rho = 0.32$ displays a distribution which is close to $P_{Wigner}(s_{re})$. At the other end is $\langle \bar{\Gamma} \rangle \rho = 8.0$, where the real parts of the resonances have lost much of their correlation (Fig. 5c). Namely, for large $\langle \bar{\Gamma} \rangle \rho$, repulsion in the complex energy plane pushes some poles apart in directions that are mainly parallel to the imaginary axis, thereby removing correlation between the real parts. The intermediate case shown in Fig. 5b is closer to $P_{Wigner}(s_{re})$ than to $P_{Poisson}(s_{re})$, but is in the regime where $P(s_{re})$ begins to deviate from $P_{Wigner}(s_{re})$ as the coupling is made stronger. Such intermediate cases can be classified by using the interpolation formula of Brody [15], which goes smoothly from one limit to the other.

Now consider two coupled manifolds with $\sigma_{bd} = 2$, as shown in Fig. 5d–f. Again, $P(s_{re})$ is examined for different values of $\langle \bar{\Gamma} \rangle \rho$. For $\langle \bar{\Gamma} \rangle \rho$ values of 0.32 and 8.0, the results are essentially the same for the one- and two-manifold cases. However, with $\langle \bar{\Gamma} \rangle \rho = 1.6$, the difference between the one- and two-manifold cases is pronounced, the former showing significant $P_{Wigner}(s_{re})$ character, while the two-manifold case resembles the result shown in Fig. 2a for two uncoupled manifolds of discrete levels. In this regime it is possible to use projections of the complex eigenenergies onto the real axis as a means

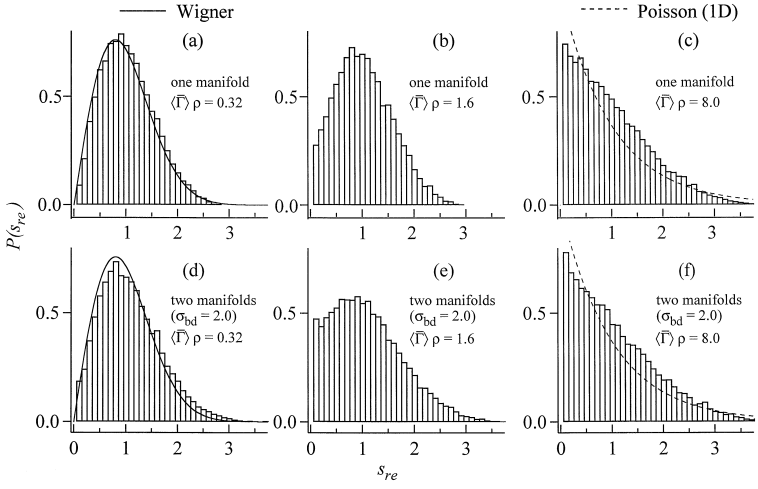


Fig. 5. Nearest-neighbor spacing distributions for the real part of the resonances, $P(s_{re})$, for two coupled manifolds with $\sigma_{bd} = 2.0$ (upper row) and one manifold (lower row) with different values of $\langle \bar{\Gamma} \rangle \rho$. The Wigner (————) and 1D Poisson (---) distributions are shown on the histograms with $\langle \bar{\Gamma} \rangle \rho = 0.32$ and $\langle \bar{\Gamma} \rangle \rho = 8.0$, respectively.

of following the evolution of the system. As the strength of the coupling to the continua increases, the system begins to behave as non-interacting manifolds.

This result can be summarized as follows. When coupling to the continuum exceeds inter-manifold coupling, photoexcited bright states decay to their continuum on a timescale which is shorter than that required for inter-manifold coupling. Thus, the appropriate density of states is that of the bright manifold, i.e. $B_2$ vibronic levels in the case of $NO_2$. On the other hand, just above reaction threshold the $B_2$ states are coupled to the dark $A_1$ states, and it is the resulting $A_1/B_2$ mixed states which decay. In this regime, coupling to the continuum is relatively weak compared to inter-manifold coupling. Note that the resonances are not overlapped in the sense that interference effects are present, although spectra terminating on levels just above $D_0$ are usually congested because different total angular momenta are accessed as per dipole selection rules.

For the case of $NO_2$ it has been discovered that the level density immediately below $D_0$ (i.e. a few $cm^{-1}$) is considerably higher than can be rationalized by combining manifolds of $A_1$ and $B_2$ vibronic symmetries [9,10,32]. It is argued that multiple PESs correlate to $O + NO$ at large interfragment separation characteristic to this regime [33], and these surfaces couple to the $A_1/B_2$ system. This increases the number of optically accessible levels and is responsible for the anomalously large threshold density of states that has been observed [33]. The numerical experiments presented above apply to this case as well. Namely, weakly coupled manifolds participate at threshold and are responsible for the small rates, whereas at higher energies coupling to the continuum recovers the $B_2$ vibronic identity of the optically excited states.

A consequence of the model is that the rate increases rapidly with energy just above $D_0$ — more so than is predicted by using transition state theory with an almost constant density of states for the narrow energy region near threshold. For example, note that the fluctuation-averaged rate in the 5 $cm^{-1}$ above $D_0$ is $\sim 2 \times 10^{10}$ $s^{-1}$ [34], whereas the threshold rate averaged over the 25 $cm^{-1}$ linewidth of the photolysis laser used in the picosecond-resolution pump-probe experiments is $1.6 \times 10^{11}$ $s^{-1}$ [35]. The difference cannot be reconciled simply by the successive openings of channels, e.g. when using PST. The density of levels that participate in the unimolecular reaction must go down. In closing, we note that similar arguments can be applied to the issue of $K$ quantum number conservation in the threshold regime [33].

## Acknowledgements

This research was supported by the National Science Foundation. The authors enjoyed and benefited from discussions with H. Reisler and M. Tuchler.

## References

[1] P.J. Robinson, K.A. Holbrook, Unimolecular Reactions (Wiley, New York, 1972).
[2] W. Forst, Theory of Unimolecular Reactions (Academic, New York, 1973).
[3] W.H. Green, C.B. Moore, W.F. Polik, Annu. Rev. Phys. Chem. 43 (1992) 591.
[4] A.E. Douglas, J. Chem. Phys. 45 (1966) 1007.
[5] R. Georges, A. Delon, R. Jost, J. Chem. Phys. 103 (1995) 1732.
[6] A. Delon, R. Jost, J. Chem. Phys. 95 (1991) 5686.
[7] A. Delon, R. Jost, M. Lombardi, J. Chem. Phys. 95 (1991) 5700.
[8] A. Delon, R. Georges, R. Jost, J. Chem. Phys. 102 (1995) 7740.
[9] R. Jost, J. Nygard, A. Pasinski, A. Delon, J. Chem. Phys. 105 (1996) 254.
[10] S.I. Ionov, H.F. Davis, K. Mikhaylichenko, L. Valachovic, B.A. Beaudet, C. Wittig, J. Chem. Phys. 101 (1994) 4809.
[11] E. Haller, L.S. Cederbaum, Chem. Phys. Lett. 101 (1983) 215.
[12] T.L. Zimmermann, L.S. Cederbaum, H.-D. Meyer, H. Köppel, J. Phys. Chem. 91 (1987) 4446.
[13] P. Pechukas, Phys. Rev. Lett. 51 (1983) 943.
[14] M.L. Mehta, Random Matrices (Academic Press, San Diego, CA, 1990).
[15] T.A. Brody, J. Flores, J.B. French, P.A. Mello, A. Pandey, S.S. Wong, Rev. Mod. Phys. 53 (1981) 385.
[16] S. Mukamel, J. Sue, A. Pandey, Chem. Phys. Lett. 105 (1984) 134.
[17] E. Haller, H. Köppel, L.S. Cederbaum, Phys. Rev. Lett. 52 (1984) 1665.
[18] E. Abramson, R.W. Field, D.I. Imre, J.L. Kinsey, J. Chem. Phys. 83 (1985) 453.
[19] W.F. Polik, D.R. Guyer, W.H. Miller, C.B. Moore, J. Chem. Phys. 92 (1990) 3471.
[20] R.L. Sundberg, E. Abramson, J.L. Kinsey, R.W. Field, J. Chem. Phys. 83 (1985) 466.

[21] E.P. Wigner, Phys. Rev. 40 (1932) 749.
[22] M.V. Berry, M. Tabor, Proc. R. Soc. Lond., Ser. A 356 (1977) 375.
[23] R. Grobe, F. Haake, H.J. Sommers, Phys. Rev. Lett. 61 (1988) 1899.
[24] V.A. Mandelshtam, H.S. Taylor, J. Chem. Soc. Farad. Trans. 93 (1997) 847.
[25] J. Ginibre, J. Math. Phys. 6 (1965) 440.
[26] H. Feshbach, Theoretical Nuclear Physics (Wiley, New York, 1992).
[27] W.F. Polik, C.B. Moore, W.H. Miller, J. Chem. Phys. 89 (1988) 3584.
[28] W.H. Miller, R. Hernandez, C.B. Moore, J. Chem. Phys. 93 (1990) 5657.
[29] U. Peskin, H. Reisler, W.H. Miller, J. Chem. Phys. 101 (1994) 9672.
[30] U. Peskin, H. Reisler, W.H. Miller, J. Chem. Phys. 102 (1995) 8874.
[31] W. John, B. Milek, H. Schanz, P. Seba, Phys. Rev. Lett. 67 (1991) 1949.
[32] J. Miyawaki, K. Yamanouchi, S. Tsuchiya, J. Chem. Phys. 99 (1993) 254.
[33] P.I. Ionov, I. Bezel, S.I. Ionov, C. Wittig, Chem. Phys. Lett. 272 (1997) 257.
[34] B. Abel, H.H. Hamann, N. Lange, J. Chem. Soc. Farad. Discuss. 102 (1997) 147.
[35] S.I. Ionov, G.A. Brucker, C. Jaques, Y. Chen, C. Wittig, J. Chem. Phys. 99 (1993) 3420.